Modelling of CaCO$_3$ Nanoparticle Formation During Overbasing of Lubricating Oil Additives

Rajdip Bandyopadhyaya,[†] R. Kumar,[‡] and K. S. Gandhi*

Department of Chemical Engineering, Indian Institute of Science, Bangalore 560 012, India

Received January 10, 2000. In Final Form: October 11, 2000

A framework of population balance equations has been developed to model formation of CaCO$_3$ nanoparticles during overbasing of lubricating oil. The process involves carbonation of a reverse micellar solution containing lime, present both in the micelles and as a suspension of lime particles in the oil. The mechanism leading to CaCO$_3$ nanoparticles in this setup consists of a number of elementary events such as CO$_2$ transport from gas to reverse micelles through the organic phase, reaction in the reverse micellar core, nucleation of CaCO$_3$, particle growth, and Brownian collisions leading to material exchange, both among reverse micellar drops and between drops and lime particles. A time scale analysis of these steps permits simplification and enables us to divide the whole process into two stages. The first consists of reaction of existing lime in micelles and a burst of nucleation of very short duration, wherein some reverse micelles beget a single nucleus each. The number of such nucleated reverse micelles depends on the relative rates of mass transfer, nucleation, and growth by intermicellar Brownian collisions. This is followed by a slow growth phase of these initial particles through Brownian collisions between nucleated reverse micelles and lime particles. The model predicts the data of Roman et al. (*J. Colloid Interface Sci.* **1991,** *144,* 324.), where on average only 10 initial reverse micelles contribute to form a CaCO$_3$ nanoparticle. A simplified version of the model, obtained in the limit of instantaneous gas transfer, is also able to approximately predict the results of Kandori et al. (*J. Colloid Interface Sci.* **1988,** *122,* 78.) where, in contrast, a huge number of 10^8 reverse micelles contribute to form one particle. The model is quite general and can be used for other gas−liquid micellar precipitation systems wherein similar relative orders of time scales are involved.

1. Introduction

Overbased lubricating oil additives aid in proper functioning of internal combustion engines. During overbasing, detergent-stabilized CaCO$_3$ nanoparticles are synthesized in situ in the lube oil, to function later as an additive. These nanoparticles inhibit acid corrosion in the engine and are required to be stable and of uniform size. The process of overbasing involves the passage of CO$_2$ gas through a hydrocarbon having a surfactant, water, and micron sized particles of Ca(OH)$_2$. The water and surfactant form swollen reverse micelles which contain Ca(OH)$_2$. On passage of CO$_2$, CaCO$_3$(l) is generated in the liquid cores of the reverse micelles which nucleate at appropriate supersaturation. These nuclei grow not only by absorption of CaCO$_3$(l) from within the micelle in which they have formed but also through coalescence (and redispersion) with other reverse micelles containing CaCO$_3$(l). Henceforth, we will use the terms micelles and reverse micelles interchangeably, while keeping in mind that we are all the time dealing with swollen reverse micelles.

Kandori et al.[1] had investigated the formation of CaCO$_3$ nanoparticles in reverse micelles containing an aqueous solution of Ca(OH)$_2$ using CaOT as surfactant. All the Ca(OH)$_2$ present in the system was in dissolved form in the reverse micelles. The precipitation was brought about by sparging CO$_2$ for a short time and subsequently desorbing CO$_2$ with N$_2$. They observed that the average particle size formed was about 100 nm and approximately 10^8 micelles contributed to the formation of each particle.

These values were quantitatively predicted by Bandyopadhyaya et al.[2] by considering the diffusion of CO$_2$ into the micelles and the reactions therein to produce supersaturation, followed by nucleation and growth of particles by collision and fusion of the micelles.

Roman et al.[3] also prepared nanoparticles of CaCO$_3$ by a slightly different procedure. These authors used as surfactant a calcium salt of a dialkyl-aryl sulfonic acid, the salt being made in situ. Methanol added as cosurfactant and water liberated during the formation of the surfactant together gave rise to reverse micelles. The Ca(OH)$_2$ was provided as *micron* sized solid particles, and a large amount of it remained unreacted after formation of the surfactant. CO$_2$ gas was passed[4] at a rate of 1.8 × 10^{-4} mol s^{-1} into the suspension of Ca(OH)$_2$ particles in the reverse micellar medium to prepare nanometer sized CaCO$_3$ particles. Under these conditions, which are superficially mildly different from those used by Kandori et al.[1] (e.g., a different surfactant, presence of Ca(OH)$_2$ particles, etc.), the authors found the nanoparticle size to be just 6 nm (against ∼100 nm of Kandori et al.[1]) and only 10 micelles to be participating in the formation of a nanoparticle (against 10^8 of Kandori et al.[1]).

The present paper proposes a generalized framework which explains the very interesting results of Roman et al.[3] The earlier model[2] used to explain the results of Kandori et al.[1] becomes a special case of the present model.

2. The Model

2.1. The Physical Process. In the process used by Roman et al.[3] before sparging of CO$_2$ is started, there are a large number of swollen reverse micelles containing Ca-

---

* To whom correspondence should be addressed. E-mail: gandhi@chemeng.iisc.ernet.in.

† Presently at Ben-Gurion University of Negev.

‡ Also at Jawaharlal Nehru Centre for Advanced Scientific Research, Bangalore.

(1) Kandori, K.; Kon-No, K.; Kitahara, A. *J. Colloid Interface Sci.* **1988,** *122,* 78.

(2) Bandyopadhyaya, R.; Kumar, R.; Gandhi, K. S.; Ramkrishna, D. *Langmuir* **1997,** *13,* 3610.

(3) Roman, J.-P.; Hoornaert, P.; Faure, D.; Biver, C.; Jacquet, F.; Martin, J. *J. Colloid Interface Sci.* **1991,** *144,* 324.

(4) Roman, J.-P. Communication through the Editor, May 2000.

(OH)$_2$ along with methanol and a small amount of water. These reverse micelles are continuously interacting with each other, fusing, redispersing, and exchanging fluid contents in the process.

The sparged CO$_2$ dissolves in the organic phase and diffuses into the swollen reverse micelles, where it reacts with the pre-existing lime. CaCO$_3$(l) thus formed attains supersaturation and may nucleate in a random way, provided the number of these molecules present in a micelle is more than the minimum required to form a stable nucleus (~5 for CaCO$_3$). Once nucleation begins, the micelles can be classified as those which have nuclei (or a nanoparticle) and those which do not. The numbers of these two will vary with time. Both receive CO$_2$ molecules and both have access to suspended Ca(OH)$_2$ particles through Brownian collisions. The processes of nucleation and growth can continue through formation of new CaCO$_3$(l) molecules in the micelles and through collisions between nucleated and non-nucleated yet supersaturated micelles, until the final particle size distribution is established at the end of the process.

The processes of particle formation and growth are significantly influenced by the collisional interactions among micelles. Depending on the rate at which micelles interact, the final results as well as the analysis of the phenomena will vary. For example, nucleation may precede all growth or nucleation as well as growth from within the micelles and through fusion with other micelles can proceed simultaneously. The latter possibility cannot be ignored a priori. For instance, after nucleation in a micelle, another micelle may fuse with it before the supersaturation has been exhausted. Such fusion can give rise to yet another nucleus in the same micelle. In such a situation, because of their strong interactions it will be necessary to consider all three processes of nucleation, growth, and fusion to determine the number of nanoparticles formed in each micelle together. If, however, the time scales for various steps are known, their comparison can lead to a specific and simpler mechanism of particle formation.

2.2. Time Scale Analysis. Analysis of time scales of various processes occurring during the formation of nanoparticles is central to the present model-building exercise. In this, we follow Bandyopadhyaya et al.,[2] who have shown how a hierarchy of time scales can be calculated to arrive at the sequence of events taking place in the semibatch reactor used by Kandori et al.[1] However, compared to Kandori et al.,[1] experiments of Roman et al.[3] involve additional processes and also some differences in process conditions, which influence the time scale analysis, and we discuss these first.

Initial Lime Content. The rate of nucleation depends on the CaCO$_3$(l) present in each micelle. The CaCO$_3$(l) molecules are formed by reaction between CO$_2$ and the lime initially present in the micelles. An additional source of formation of CaCO$_3$(l) molecules is through the reaction between CO$_2$ and Ca(OH)$_2$ picked up by micelles, unsaturated with respect to Ca(OH)$_2$, when they collide with the solid lime particles. At saturation conditions, on the average, a molecule of Ca(OH)$_2$ is present in about 15 micelles. Thus, we do not expect this additional source of CaCO$_3$(l) to be activated till almost all the initially present lime is exhausted by reaction, and we expect collisions between the micelles containing Ca(OH)$_2$ molecules and the solid lime particles to be infructuous. The initial lime content of the micelles is therefore needed to make estimates of the nucleation rates. The amount of Ca(OH)$_2$ present initially in the micelles has been calculated in two different ways. Roman et al.[3] provide a size estimate
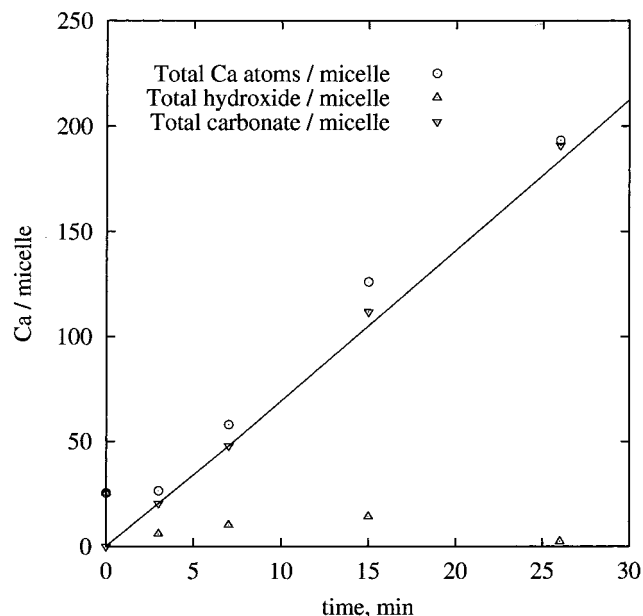

Figure 1. Experimental observations of Roman et al. (ref 3) on lime and carbonate contents in the system. The straight line is through the points representing carbonate content and has a slope of 0.118 s^{-1}.

of 7.2 Å for the CaCO$_3$ particle, which would have formed in a single micelle, if only the amount of lime present in a single micelle was used in its making. The size is equivalent to 25 molecules of carbonate being present in the particle. Thus, initially 25 molecules of Ca(OH)$_2$ would have been present in each micelle. The same value of 25 Ca(OH)$_2$ molecules per micelle is also obtained from small-angle X-ray scattering measurements[3] of the initial sizes of micelles prepared under different conditions. We use this figure in our calculations.

If all lime molecules are in dissolved form, the concentration of Ca(OH)$_2$ present in the micelles at the beginning is considerably high, approximately 400 times the bulk solubility in the micellar core. Although there exist reports in the literature on enhanced solubility of many solutes in micellar water because of its altered state, the enhancements are modest, being of the order of 5−7 times (e.g., for poorly soluble protein in Matzke et al.[5]). We do not address the question of the form in which Ca(OH)$_2$ is present. We merely assume that the following reaction occurs inside the micelle whenever Ca(OH)$_2$ and CO$_2$ are present together:

$$Ca(OH)_2 + CO_2 = CaCO_3(l) + H_2O$$
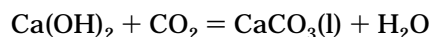
Solubilization of Lime. Roman et al.[3] reported experimental data on the amount of lime and carbonate present in the micelles as a function of time. The data are shown in Figure 1. The average carbonate content in a micelle is observed to increase linearly with time at a rate of 0.118 molecules per second. However, the Ca(OH)$_2$ present in the micelles falls very rapidly from the initial value and is rather small at 3 min itself, but from then on it shows a slow and marginal rise until 15 min and then rapidly falls to negligible levels at 26 min. Against this is the entry of CO$_2$ into the system at a rate of 1.8 × 10^{-4} mol s^{-1}, or 0.112 molecules into a micelle per second, which is nearly the same as the rate at which the carbonate content in a micelle increases. It can therefore be concluded

(5) Matzke, S. F.; Creagh, A. L.; Haynes, C. A.; Prausnitz, J. M.; Blanch, H. W. *Biotechnol. Bioeng.* **1992**, *40*, 91.

Table 1. Time Scales of Roman et al.[a]

event	formula	time scale (s)
mass transfer entry of one CO_2 molecule (τ_m)	$1/k_g$	10
reaction of a CO_2 molecule with lime (τ_r)[b]	$1/k_1[OH^-]$	10^{-5}
collision−fusion with any micelle (τ_c)	$1/\beta_m q_m N_0^{(0)}$	10^{-1}
nucleation of $CaCO_3$ particle in a micelle (assuming only MeOH in core) ($\tau_n^{(m)}$)	$1/k_n(k)$	10^{-1}
nucleation of $CaCO_3$ particle in unit volume of system ($\tau_{nn}^{(m)}$)	$1/k_n(k)N_0^{(0)}$	10^{-17}
growth of a $CaCO_3$ particle inside a micelle (τ_g)	$V_{mic}(1/q)$	10^{-10}
Ca(OH)₂ pickup by micelle−particle collision and solubilization (τ_{cp})	$1/\beta_p q_p N_p^{(0)}$	10
collision−fusion with a nucleated micelle (τ_{cn})	$1/\beta_m q_m N_1^{(0)}$	1

[a] Reference 3. [b] $k_1 = 6000$ L mol⁻¹ s⁻¹ is the reported rate constant for the reaction $CO_2 + [OH^-] \rightarrow HCO_3^-$. See: Danckwerts, P. V. *Gas-Liquid Reactions*; McGraw-Hill Book Company: New York, 1970; p 239.

that all the CO_2 is absorbed by the organic phase and reacts completely. Further, in view of the steady increase in the carbonate content, the very small increase in the Ca(OH)₂ content shows that the rate of CO_2 entry is also approximately balanced by the rate of entry of Ca(OH)₂ molecules through collisions between micelles and solid lime particles from about 3 min onward. We therefore assume a linear trend for the pickup of lime by micelles. However, the very steep drop in the lime content seen in the experimental data between 0 and 3 min suggests that lime pickup is possible only after exhaustion of the initial lime content. We implement this by assuming that micelles become unsaturated with respect to lime after complete reaction of the initial lime and that, from then on, each time an unsaturated micelle collides with a solid lime particle, a molecule of lime can enter it with an efficiency β_p, which has been determined to stoichiometrically match the experimental rate of sparging of CO_2. The value of β_p turns out to be equal to 0.055 after assuming that the solid lime particles are 1 μm in size.

Relative Rates of Events. To arrive at the sequence of events and to compare their relative rates, we list the various events in the process that involve a micelle in Table 1 along with the associated time scales. The values of the time scales listed are equal to the reciprocal of the rates of the corresponding processes.

(i) Mass transfer versus reaction rate: Comparison of the time scales of mass transfer (τ_m and τ_{cp}) and reaction (τ_r) shows that both the rate of entry of CO_2 molecules into a micelle and the rate of pickup of lime by micelles are very much slower than the rate at which they react. So, in our model we assume that CO_2 reacts instantaneously with lime in the micelle. Further, both τ_m and τ_{cp} are larger than τ_c, indicating that even if CO_2 is absorbed by a micelle which does not contain Ca(OH)₂ molecules it gets redistributed rapidly and reacts with lime present in some other micelle. We therefore have eliminated any calculation of chemical reaction rates and equated the entry rate of CO_2 to the formation rate of $CaCO_3(l)$, *as long as lime is present inside the micelles.*

(ii) Nucleation rate versus growth rate: The concentration of $CaCO_3(l)$ in micelles increases because of the reaction between lime and CO_2. We estimate two time scales associated with nucleation. One is the average time taken between two nuclei formed in a single micelle ($\tau_n^{(m)}$), if supersaturation inside remains uniform at a particular level. The second is the time scale over which nucleation

occurs per unit volume of the total liquid present in the system, $\tau_{nn}^{(m)}$. The latter is an overall nucleation time scale and will be discussed a little later. The time scale of nucleation in a single micelle ($\tau_n^{(m)}$), containing the minimum number required to nucleate, five molecules of $CaCO_3(l)$, is 10^{-1} s. It has been calculated on the basis of the solubility of $CaCO_3$ in methanol, because essentially only methanol is present in the micelles in the beginning.

As CO_2 is passed, new $CaCO_3(l)$ molecules are generated in the micelle, if unreacted lime exists. For a nucleated micelle, the new carbonate molecules can be used up either for particle growth or for generating a second nucleus. If the growth rate is less than the nucleation rate in the micelle, one can have more than one nucleus born in the same micelle. If, on the other hand, the growth rate is much higher, then the additional molecule adds to the size of the particle without generating an extra nucleus in the micelle.

Even when growth is fast enough to consume the excess molecules present in the micelle after the first nucleus is formed, there exists another way in which the nucleated micelle can have more than one nucleus. All micelles undergo collision and fusion with other micelles in the medium. When a nucleated micelle fuses with a non-nucleated micelle having a sufficient number of $CaCO_3(l)$ molecules, two alternative events can occur in the transient dimer: either the newly acquired carbonate molecules are incorporated in the existing $CaCO_3$ particle via growth or, in view of the attendant buildup of supersaturation in the original mononucleated micelle, a second nucleus is born in it. Here also, relative rates of nucleation and growth decide whether the increased supersaturation would result in an additional nucleus or growth of the existing nucleus. Thus, we need to compare the nucleation and growth time scales to decide whether a nucleated micelle can have two or more nuclei.

In Table 1, it is seen that $\tau_n^{(m)}$ is far higher than the growth time scale, τ_g. This would imply that once a nucleus is formed, it exhausts the supersaturation by growth before another nucleus can be produced, both when the first nucleus is formed and also when the nucleated micelle coalesces with a supersaturated micelle. It is further seen that $\tau_g \ll \tau_c$, implying the growth of a $CaCO_3$ particle inside a micelle to be much faster than the collision time of that particular micelle with other non-nucleated but supersaturated micelles. This prevents further buildup of supersaturation in a nucleated micelle. Similarly, $\tau_g \ll \tau_m$ or τ_{cp}. Together, these comparisons imply that if a nucleated micelle develops supersaturation, either by collision−fusion with a non-nucleated but supersaturated micelle or by intake of CO_2 or lime, it is instantaneously dissipated by very fast particle growth. Two conclusions can therefore be drawn. First, each micelle can at best have only one particle. Second, any $CaCO_3(l)$ formed in a nucleated micelle is incorporated by growth into the existing $CaCO_3$ particle, and growth is completed before any other process can affect the micellar state. In fact, τ_g is the smallest of all time scales involving a micelle, and hence growth may be treated as instantaneous. Its dynamics does not have to be specifically incorporated in the analysis. It occurs in discrete amounts at specific instants, as and when supersaturation in a nucleated micelle gets generated.

The high rate at which supersaturation is absorbed by a nanoparticle has a very important, though indirect, effect on the *overall nucleation rate* in the entire system, which determines the total number of nanoparticles formed in the process. When a micelle containing $CaCO_3(l)$ collides

with a micelle containing a particle, all the $CaCO_3(l)$ is absorbed by the particle instantaneously. As a result, the average concentration of $CaCO_3(l)$ in the system is lowered. The rate of nucleation in the entire system is given by the rate of nucleation in a micelle that contains at least the five molecules required to form a nucleus multiplied by the fraction of micelles containing that many molecules. The latter is proportional to the average concentration of $CaCO_3(l)$ in the system, and the relationship will be discussed shortly. However, to get a feel for the number we give an estimate. The overall nucleation time scale, $\tau_n^{(m)}$, is of the order of 10^{-17} s for Roman et al.[3] if we assume that the mean $CaCO_3(l)$ content in a micelle is unity, and the Poisson distribution holds. If the mean population of $CaCO_3(l)$ is 0.5, the above time scale increases by a factor of 50. The mean population thus plays an important role and can be determined only by a model.

(iii) Rate of intermicellar exchange of $CaCO_3(l)$: The state of non-nucleated micelles, characterized in terms of $CaCO_3(l)$, evolves by acquiring $CaCO_3(l)$ molecules through reaction. It starts from zero molecules and builds up to a level at which nucleation can occur. Apart from nucleation, it can also decrease because of the simultaneous loss of $CaCO_3(l)$ molecules when collision with nucleated micelles occurs. Finally, the state is also affected when Brownian collisions take place among non-nucleated micelles, rendering redistribution of the $CaCO_3(l)$ molecules.

From Table 1, we find that τ_c, which is indicative of the time scale in which $CaCO_3(l)$ molecules are redistributed in the non-nucleated micelles, is less than the time scales of two other events affecting a non-nucleated micelle, τ_{cn} and τ_{cp}. Rearrangement of carbonate molecules in non-nucleated micelles thus being very fast when compared to other relevant processes, it is reasonable to assume that the distribution of $CaCO_3(l)$ molecules in these micelles is given by Poisson statistics. To calculate the Poisson distribution, we need to specify only the first two moments, namely, the number of non-nucleated micelles and the total number of carbonate molecules in them. The whole hierarchy of higher moment equations then follows from the definition of the Poisson distribution. This then obviates the need to use a population balance equation for non-nucleated micelles in terms of $CaCO_3(l)$ molecules.

The results of the time scale analysis will lead to simplifications in the model development, as will be shown in section 2.4. Before discussing those, we propose the following mechanism for the process.

2.3. Proposed Mechanism of Overbasing. Though τ_m and τ_{cp} are similar in magnitude, solubilization of lime from particles can occur only when the initially existing $Ca(OH)_2$ in the micelles is exhausted and the micelles become unsaturated with respect to lime. Therefore, lime particles suspended in oil would not contribute to reaction, nucleation, or growth during this initial phase. Only after reaction exhausts the initial lime present in the micelles can further solubilization from lime particles take place. Additional $CaCO_3(l)$ generated by reaction between CO_2 and lime solubilized in this manner contributes toward the growth of existing nanoparticles and possibly to the nucleation of new particles. The whole process of overbasing therefore may be divided into two distinct phases as summarized below.

Phase I is the period of nucleation and growth of $CaCO_3$ particles formed from the 25 molecules of $Ca(OH)_2$ initially present in each micelle. During this phase, new particles are formed by nucleation and instantaneous growth by absorption of supersaturation present in the micelle. Further growth of the particle may also occur because of

coalescence between micelles containing $CaCO_3(l)$. As mentioned earlier, this type of growth has an adverse effect on nucleation. Phase I continues until the lime initially present in the micelles is converted into carbonate, present mostly as $CaCO_3$ nanoparticles and a few $CaCO_3(l)$ molecules. So, the end of phase I occurs when the micelles do not contain any residual lime from that present at the beginning, thus making them unsaturated with respect to $Ca(OH)_2$ and capable of picking up lime from the solid particles.

Phase II mostly is a growth phase of particles formed during phase I. In this phase, $Ca(OH)_2$ comes into the micelles from the lime particles and CO_2 comes from the gas being sparged. The $CaCO_3(l)$ formed contributes primarily to the increase in the size of the existing nanoparticle. The lime is picked up because of particle–micelle collisions, the efficiency of which has been adjusted to match the observation that solubilized lime reacts with the incoming CO_2 without accumulating; that is, the rates of entry of CO_2 and solubilization of $Ca(OH)_2$ are matched stoichiometrically. Thus in phase II, particles formed in phase I grow and add to their size with marginal nucleation. The result is the formation of a large number of relatively uniform sized particles.

The entire process of particle formation and growth is depicted in Figure 2. The schematic shows the sequence of steps a typical micelle can undergo starting from initially present lime. While supersaturation in the micelle builds up, it can collide with a nucleated micelle. Otherwise, it can nucleate after attaining the critical number of molecules. The nucleated micelle can further grow by absorption of CO_2 or lime as well as through collision with non-nucleated yet supersaturated micelles. The final number of particles formed is dictated by the delicate balance among the rate of formation of $CaCO_3(l)$, the rate of nucleation, and the rate of growth of nanoparticles by *collision–fusion* processes.

2.4. Number Densities. We have two kinds of micelles: the nucleated ones containing nanoparticles of $CaCO_3$ and the non-nucleated ones, containing dissolved $CaCO_3(l)$. Our interest is in the variation of their numbers with time and also in the distribution of calcium carbonate molecules therein. To this end, we start with two general number density functions $n_0^+(i,j,l,t)$ and $n_1^+(i,j,k,t)$ for non-nucleated and nucleated micelles, respectively. $n_0^+(i,j,l,t)$ is the number of non-nucleated micelles per unit volume of the system, which at time t contain i $Ca(OH)_2$ molecules, j CO_2 molecules, and l $CaCO_3(l)$ molecules. Correspondingly, $n_1^+(i,j,k,t)$ denotes the number of nucleated micelles per unit volume at time t, containing a $CaCO_3$ particle having k molecules.

In phase I, the incoming CO_2 molecules react instantaneously on entering a micellar drop, because of the presence of a significant amount of $Ca(OH)_2$, leaving no free CO_2 and implying $j = 0$. Similarly, throughout phase II both i and j are equal to 0, because $Ca(OH)_2$ and CO_2 are supplied in stoichiometric ratio and react instantaneously. Because i is in excess and $j = 0$ in phase I and both i and j are equal to 0 in phase II, there is no need to keep track of populations of i and j in individual micelles. This results in simpler number density functions. Thus, we now have $n_0(l, t)$ and $n_1(k, t)$ as the number of micelles containing l molecules of $CaCO_3(l)$ and k molecules of $CaCO_3$ in non-nucleated and nucleated micelles, respectively, per cm^3 of the dispersion at time t. Phase I begins with $n_1(k,t)$ being zero for all k and only $n_0(0,t)$ being nonzero. This phase ends when the total molecules of
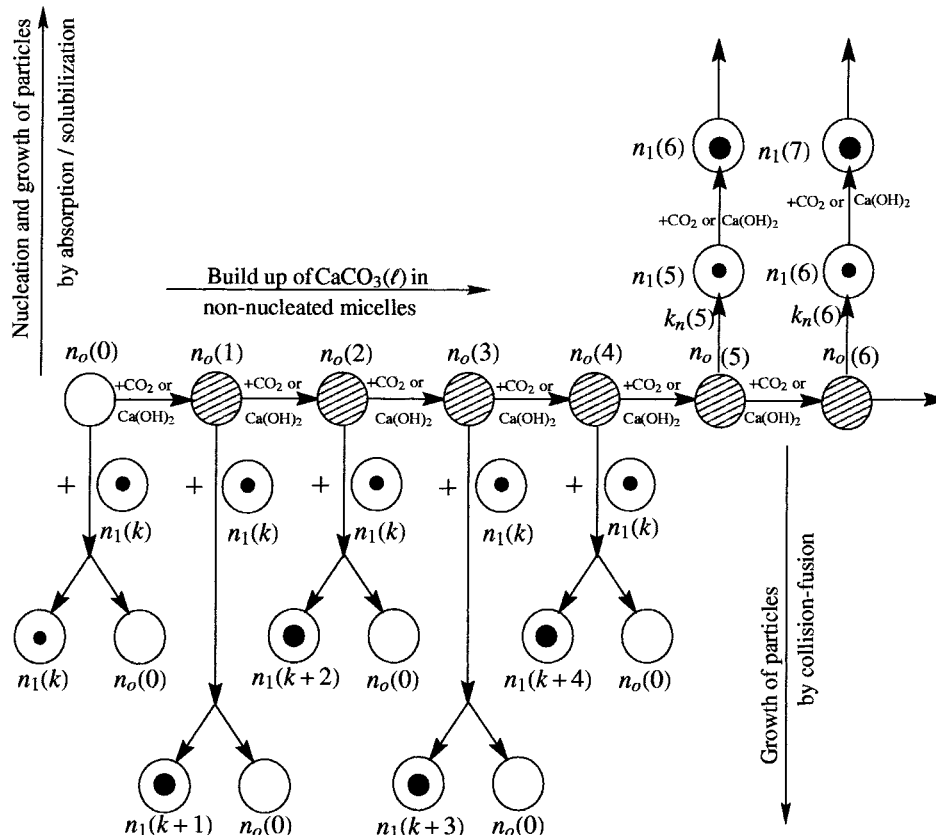
Figure 2. Schematic of the assumed overbasing process in phase I and phase II. The buildup of supersaturation is due to intake of CO_2 in phase I and intake of CO_2 and $Ca(OH)_2$ in phase II.

CaCO₃ present in the system equals the total molecules of $Ca(OH)_2$ initially present in the micelles.

The total number of nucleated and non-nucleated micelles can be expressed in terms of these number densities as follows:

$$N_1^{(0)}(t) = \sum_{k=k_c}^{\infty} n_1(k,t) \tag{1}$$

$$N_0^{(0)}(t) = \sum_{l=0}^{\infty} n_0(l,t) \tag{2}$$

We have started with $k = k_c$ for the sum, because at least the critical number of CaCO₃(l) molecules (k_c) is required for nucleation to occur. The superscript indicates that it is the zeroth moment.

2.5. Distribution of CaCO₃(l) in Non-nucleated Micelles. As indicated earlier, the population of CaCO₃(l) molecules in the micelles attain Poisson distribution because of extremely fast coalescence and redispersion among micelles. If $P_l(t)$ is the probability that l number of CaCO₃(l) molecules are present in a non-nucleated micelle, then

$$n_0(l,t) = N_0^{(0)}(t) \, P_l(t) \qquad l = 0, 1, 2, 3... \tag{3}$$

From the Poisson distribution then, $P_l(t)$ is given by

$$P_l(t) = \frac{\bar{l}(t)^l \exp[-\bar{l}(t)]}{l!} \qquad l = 0, 1, 2, 3... \tag{4}$$

In the above, $\bar{l}(t)$ is the average number of CaCO₃(l) molecules present in a non-nucleated micelle at any given time and is given by $N_0^{(1)}(t)/N_0^{(0)}(t)$, the ratio of first to zeroth moments. Thus, solution of eq 4 requires the knowledge of $N_0^{(0)}(t)$ as well as $N_0^{(1)}(t)$. As fusion and fission do not change the total number of non-nucleated micelles, it can decrease only because of nucleation events. Thus $N_0^{(0)}(t)$ is given by the following equation:

$$\frac{dN_0^{(0)}(t)}{dt} = -\sum_{l=k_c}^{\infty} k_n(l) \, n_0(l,t) \tag{5}$$

where the right-hand side gives the rate of nucleation. The equation for $N_0^{(1)}(t)$, which gives the total number of CaCO₃(l) molecules in the micelles is given below.

$$\frac{dN_0^{(1)}(t)}{dt} = -\sum_{l=k_c}^{\infty} l k_n(l) \, n_0(l,t) - \beta_m q_m N_1^{(0)}(t) \, N_0^{(1)}(t) + k_g N_0^{(0)}(t) \tag{6}$$

The first two terms on the right-hand side indicate the rate at which $N_0^{(1)}(t)$ is decreasing: the first one because of nucleation and the second because of coalescence with nucleated micelles. We have shown previously that entry of CO_2 is controlling in phase I, and pickup of $Ca(OH)_2$ as well as supply of CO_2 are equal in phase II. Hence, either can be treated as the controlling step in phase II. We will present the equations in a form in which availability of $Ca(OH)_2$ is made the controlling step, which yields a different last term in eq 6 for phase II. This is done because if the rate of sparging of CO_2 is increased, solubilization

of lime from solid particles can become controlling in phase II. Hence, to make the model applicable to more general situations (including other systems as well as higher gas flow rates), the more complex case of the solubilization rate controlled process has been presented in the equations. Generation of new $CaCO_3(l)$ molecules by reaction of lime with CO_2 in phase I is indicated by the last term in eq 6. Thus, for phase II k_g in the equation would be replaced by $\beta_p q_p N_p^{(0)}$.

This equation clearly indicates the importance of the balance between rates of collisional growth of particles, nucleation, and rate of formation of $CaCO_3(l)$. If $\beta_m q_m$ is large, then even for small values of $N_1^{(0)}$, that is, even when a small fraction of micelles nucleate, $\beta_m q_m N_1^{(0)} N_0^{(1)}$ can exceed $k_g N_0^{(0)}$. From then on, the mean population of $CaCO_3(l)$ in the micelles decreases. Hence, formation of new particles stops, and the existing particles will grow, absorbing all the $CaCO_3(l)$ forming in the system. Hence, a smaller number of particles are formed as the rate of collisional growth of particles outstrips the rate of formation of $CaCO_3(l)$.

2.6. Distribution of CaCO$_3$ in Nucleated Micelles. As nucleated micelles cannot exchange $CaCO_3$ nanoparticles through collision, the Poisson distribution is not applicable here. Hence, we have to make use of population balance equations and obtain moment equations from them. Therefore, we first write number balance equations for micelles containing critical sized nuclei and those containing more than critical, for phase I and phase II.

Phase I:

$$\frac{dn_1(k_c,t)}{dt} = k_n(k_c)\, n_0(k_c,t) - $$
$$\beta_m q_m\, n_1(k_c,t)\, N_0^{(0)}(t) \sum_{l=1}^{\infty} P_l(t) - k_g\, n_1(k_c,t) \quad (7)$$

$$\frac{dn_1(k,t)}{dt} = k_n(k)\, n_0(k,t) - \beta_m q_m\, n_1(k,t)\, N_0^{(0)}(t) \sum_{l=1}^{\infty} P_l(t) + $$
$$\beta_m q_m \sum_{l=1}^{k-k_c} n_1(k-l,t)\, n_0(l,t) - k_g\, n_1(k,t) + k_g\, n_1(k-1,t)$$
$$k = k_c + 1,\ k_c + 2,\ k_c + 3... \quad (8)$$

Phase II:

$$\frac{dn_1(k_c,t)}{dt} = k_n(k_c)\, n_0(k_c,t) - $$
$$\beta_m q_m\, n_1(k_c,t)\, N_0^{(0)}(t) \sum_{l=1}^{\infty} P_l(t) - \beta_p q_p N_p^{(0)}\, n_1(k_c,t) \quad (9)$$

$$\frac{dn_1(k,t)}{dt} = k_n(k)\, n_0(k,t) - \beta_m q_m\, n_1(k,t)\, N_0^{(0)}(t) \sum_{l=1}^{\infty} P_l(t) + $$
$$\beta_m q_m \sum_{l=1}^{k-k_c} n_1(k-l,\ t)\, n_0(l,t) - \beta_p q_p N_p^{(0)}\, n_1(k,t) + $$
$$\beta_p q_p N_p^{(0)}\, n_1(k-1,t)$$
$$k = k_c + 1,\ k_c + 2,\ k_c + 3... \quad (10)$$

The first term on the right-hand side of eqs 8 and 10 gives the generation of nucleated micelles having a particle containing k $CaCO_3$ molecules. The second term represents loss due to growth of the particle of k molecules, when fusion with any carbonate containing non-nucleated

micelle occurs. In contrast, the third term accounts for gain due to formation of a micelle containing a particle of k molecules during fusion between a nucleated and a non-nucleated micelle of appropriate carbonate contents. Similarly, the last two terms in these two equations represent loss and gain of nucleated micelles, respectively, because of particle growth, the loss and gain being due to CO_2 absorption in phase I and by way of lime solubilization in phase II.

The number of micelles containing a particle and the average size of the particle in terms of the number of $CaCO_3$ molecules k need to be calculated from the model, for the purposes of comparison with the experimental observations. These can be derived from the zeroth and first moments of eqs 7–10, whereas standard deviation requires the corresponding second moment. In general, the nth moment is given by

$$N_1^{(n)}(t) = \sum_{k=k_c}^{\infty} k^n\, n_1(k,t) \qquad n = 0,\ 1,\ 2,\ 3... \quad (11)$$

A similar expression can also be written for non-nucleated micelles. The equations for the moments are given below.

The equation for the zeroth moment of nucleated micelles $N_1^{(0)}(t)$, giving the total number of nucleated micelles, is

$$\frac{dN_1^{(0)}(t)}{dt} = \sum_{l=k_c}^{\infty} k_n(l)\, n_0(l,t) \quad (12)$$

The average size of the particle can be calculated from the average number of carbonate molecules contained in a nucleated particle. The first moment of nucleated micelles is required for this purpose, and for phase I it is given by

$$\frac{dN_1^{(1)}(t)}{dt} = \sum_{l=k_c}^{\infty} l k_n(l)\, n_0(l,t) + $$
$$\beta_m q_m N_1^{(0)}(t)\, N_0^{(1)}(t) + k_g N_1^{(0)}(t) \quad (13)$$

The first term on the right-hand side of the above equation represents nucleation, and the second term gives collisional growth. The last term implies growth due to CO_2 absorption and subsequent reaction. During phase II, this term is replaced by growth due to lime pickup and reaction, whence k_g is substituted by $\beta_p q_p N_p^{(0)}$.

We need the second moment of nucleated micelles for estimating standard deviation in particle size, which is given by the following equation in phase I:

$$\frac{dN_1^{(2)}(t)}{dt} = \sum_{l=k_c}^{\infty} l^2\, k_n(l)\, n_0(l,t) + \beta_m q_m[2N_0^{(1)}(t)\, N_1^{(1)}(t) + $$
$$N_0^{(2)}(t)\, N_1^{(0)}(t)] + k_g[2N_1^{(1)}(t) + N_1^{(0)}(t)] \quad (14)$$

The last two moment equations have been obtained directly from the population balance eqs 7–10. As usual in phase II, k_g is replaced by $\beta_p q_p N_p^{(0)}$.

Combining eqs 5 and 12, we note that the rate of change of the total number of micelles in the system is zero, as assumed in the physical mechanism. Also, on adding eqs 6 and 13 we find the total rate of formation of carbonate molecules (including liquid and solid forms) is $k_g[N_0^{(0)}(t) + N_1^{(0)}(t)]$ in phase I and $\beta_p q_p N_p^{(0)}[N_0^{(0)}(t) + N_1^{(0)}(t)]$ in phase II.

2.7. Balance for Ca(OH)₂. Having considered the balance for distribution of carbonate molecules over the nucleated and non-nucleated micelles, we need to write down the balance for obtaining the total number of Ca-(OH)₂ molecules in the micelles. This would determine when the model equations have to be changed from phase I to phase II. Initially, the simulation starts with 25 Ca-(OH)₂ molecules per micelle, which continuously decreases during phase I. Once this number decreases to zero, the solution is based on model equations of phase II. The changeover is tracked by the following equation, whose right-hand side represents loss of lime via reaction.

$$\frac{\mathrm{d}N^{(1)}_{\mathrm{Ca(OH)_2}}(t)}{\mathrm{d}t} = -k_{\mathrm{g}}[N^{(0)}_0(t) + N^{(0)}_1(t)] = -k_{\mathrm{g}} \quad (15)$$

Thus, phase I lasts while $k_{\mathrm{g}}t \le 25$. Because the increase in lime molecules resulting from pickup by collisions with solid Ca(OH)₂ particles is stoichiometrically balanced by the loss due to very fast reaction with CO₂, the left-hand side is equal to zero in phase II.

2.8. Nondimensionalization and Moment Equations. To compare with the experimental data of Roman et al.,[3] the number density and moments are normalized with the initial number of micelles, $N^{(0)}_0(0)$. The nondimensional number density function of non-nucleated micelles is hence given by

$$\bar{n}_0(l,\tau) = \frac{n_0(l,t)}{N^{(0)}_0(0)} \quad (16)$$

where $N^{(0)}_0(0) = n_0(0,t{=}0)$.

The nondimensional moments are then defined as follows.

$$\mu^{(n)}_1(\tau) = \frac{N^{(n)}_1(t)}{k^n_{\mathrm{c}} N^{(0)}_0(0)} \qquad n = 0, 1, 2, 3... \quad (17)$$

$$\mu^{(n)}_0(\tau) = \frac{N^{(n)}_0(t)}{k^n_{\mathrm{c}} N^{(0)}_0(0)} \qquad n = 0, 1, 2, 3... \quad (18)$$

where

$$\tau = k_{\mathrm{g}}t \quad (19)$$

is nondimensional time.

The nondimensional number of the suspended, micron-sized lime particles remains unchanged during the whole process as only the particle size reduces because of progressive dissolution. This constant number is given as

$$\mu^{(0)}_{\mathrm{p}} = \frac{N^{(0)}_{\mathrm{p}}}{N^{(0)}_0(0)} \quad (20)$$

The total number of molecules in the lime particles in nondimensional form is expressed as

$$\mu^{(1)}_{\mathrm{p}}(\tau) = \frac{N^{(1)}_{\mathrm{p}}(t)}{N^{(0)}_0(0)} \quad (21)$$

The total number of molecules of Ca(OH)₂ in the micelles, at any instant, in nondimensional form is given by

$$\mu^{(1)}_{\mathrm{Ca(OH)_2}}(\tau) = \frac{N^{(1)}_{\mathrm{Ca(OH)_2}}(t)}{k_{\mathrm{c}} N^{(0)}_0(0)} \quad (22)$$

Two nondimensional parameters appear in the system of equations which characterize the relative rates of inter-micellar exchange due to Brownian coalescence to the nucleation rate (at the critical number of molecules) on one hand and the frequency of lime pickup by micelle–particle Brownian collisions to the nucleation rate on the other hand.

$$\Omega(k_{\mathrm{c}}) = \frac{\beta_{\mathrm{m}} q_{\mathrm{m}} N^{(0)}_0(0)}{k_{\mathrm{n}}(k_{\mathrm{c}})} \quad (23)$$

$$\Omega_{\mathrm{p}}(k_{\mathrm{c}}) = \frac{\beta_{\mathrm{p}} q_{\mathrm{p}} N^{(0)}_0(0)}{k_{\mathrm{n}}(k_{\mathrm{c}})} \quad (24)$$

Another important parameter is $\zeta(l)$, denoting the ratio of the nucleation rate in a micelle having l CaCO₃ molecules to its absorption rate of CO₂ by mass transfer.

$$\zeta(l) = \frac{k_{\mathrm{n}}(l)}{k_{\mathrm{g}}} \quad (25)$$

The nondimensional moment equations are now written in the following fashion. All the dependent variables are understood to be functions of τ. In phase I, the equations take the following form.

$$\frac{\mathrm{d}\mu^{(0)}_1}{\mathrm{d}\tau} = \sum_{l=k_{\mathrm{c}}}^{\infty} \zeta(l)\, \bar{n}_0(l,\tau) \quad (26)$$

$$\frac{\mathrm{d}\mu^{(1)}_1}{\mathrm{d}\tau} = \sum_{l=k_{\mathrm{c}}}^{\infty} \frac{l}{k_{\mathrm{c}}} \zeta(l)\, \bar{n}_0(l,\tau) + \\ \zeta(k_{\mathrm{c}})\, \Omega(k_{\mathrm{c}})\, \mu^{(1)}_0(\tau)\, \mu^{(0)}_1(\tau) + \frac{\mu^{(0)}_1(\tau)}{k_{\mathrm{c}}} \quad (27)$$

$$\frac{\mathrm{d}\mu^{(2)}_1}{\mathrm{d}\tau} = \sum_{l=k_{\mathrm{c}}}^{\infty} \left(\frac{l}{k_{\mathrm{c}}}\right)^2 \zeta(l)\, \bar{n}_0(l,\tau) + \zeta(k_{\mathrm{c}})\, \Omega(k_{\mathrm{c}})[2\mu^{(1)}_0(\tau)\, \mu^{(1)}_1(\tau) + \\ \mu^{(2)}_0(\tau)\, \mu^{(0)}_1(\tau)] + \frac{1}{k_{\mathrm{c}}}\left[2\mu^{(1)}_1(\tau) + \frac{1}{k_{\mathrm{c}}}\mu^{(0)}_1(\tau)\right] \quad (28)$$

$$\frac{\mathrm{d}\mu^{(0)}_0}{\mathrm{d}\tau} = -\frac{\mathrm{d}\mu^{(0)}_1}{\mathrm{d}\tau} \quad (29)$$

$$\frac{\mathrm{d}\mu^{(1)}_0}{\mathrm{d}\tau} = -\sum_{l=k_{\mathrm{c}}}^{\infty} \frac{l}{k_{\mathrm{c}}} \zeta(l)\, \bar{n}_0(l,\tau) - \\ \zeta(k_{\mathrm{c}})\, \Omega(k_{\mathrm{c}})\, \mu^{(1)}_0(\tau)\, \mu^{(0)}_1(\tau) + \frac{\mu^{(0)}_0(\tau)}{k_{\mathrm{c}}} \quad (30)$$

$$\frac{\mathrm{d}\mu^{(1)}_{\mathrm{Ca(OH)_2}}}{\mathrm{d}\tau} = -\frac{1}{k_{\mathrm{c}}} \quad (31)$$

In phase II, the equations become

$$\frac{\mathrm{d}\mu^{(0)}_1}{\mathrm{d}\tau} = \sum_{l=k_{\mathrm{c}}}^{\infty} \zeta(l)\, \bar{n}_0(l,\tau) \quad (32)$$

$$\frac{d\mu_1^{(1)}}{d\tau} = \sum_{l=k_c}^{\infty} \frac{l}{k_c} \zeta(l)\, \bar{n}_0(l,\tau) + \zeta(k_c)\, \Omega(k_c)\, \mu_0^{(1)}(\tau)\, \mu_1^{(0)}(\tau) +$$
$$\frac{\zeta(k_c)\, \Omega_p(k_c)\, \mu_p^{(0)}}{k_c} \mu_1^{(0)}(\tau) \quad (33)$$

$$\frac{d\mu_1^{(2)}}{d\tau} = \sum_{l=k_c}^{\infty} \left(\frac{l}{k_c}\right)^2 \zeta(l)\, \bar{n}_0(l,\tau) + \zeta(k_c)\, \Omega(k_c) \times$$
$$[2\mu_0^{(1)}(\tau)\, \mu_1^{(1)}(\tau) + \mu_0^{(2)}(\tau)\, \mu_1^{(0)}(\tau)] +$$
$$\frac{\zeta(k_c)\, \Omega_p(k_c)\, \mu_p^{(0)}}{k_c}\left[2\mu_1^{(1)}(\tau) + \frac{1}{k_c}\mu_1^{(0)}(\tau)\right] \quad (34)$$

$$\frac{d\mu_0^{(0)}}{d\tau} = -\frac{d\mu_1^{(0)}}{d\tau} \quad (35)$$

$$\frac{d\mu_0^{(1)}}{d\tau} = -\sum_{l=k_c}^{\infty} \frac{l}{k_c} \zeta(l)\, \bar{n}_0(l,\tau) - \zeta(k_c)\, \Omega(k_c)\, \mu_0^{(1)}(\tau)\, \mu_1^{(0)}(\tau) +$$
$$\frac{\zeta(k_c)\, \Omega_p(k_c)\, \mu_p^{(0)}}{k_c}\mu_0^{(0)}\tau \quad (36)$$

$$\frac{d\mu_{Ca(OH)_2}^{(1)}}{d\tau} = 0 \quad (37)$$

The process of dissolution of solid lime begins only in phase II and continues until 26 min when 95% of the lime is exhausted.[4] This can be followed by solving the above equations till the specified value of time is reached.

The moment eqs 28 and 34 contain $\mu_0^{(2)}(\tau)$, which is the dimensionless second moment of $n_0(l, t)$. For the Poisson distribution, the second moment is the sum of the variance and square of the first moment, and the variance is same as its mean. Thus, we obtain $\mu_0^{(2)}(\tau)$ as follows.

$$\mu_0^{(2)}(\tau) = \frac{\mu_0^{(0)}(\tau)}{k_c^{\,2}}[\bar{l}(\tau) + \bar{l}^2(\tau)] \quad (38)$$

where

$$\bar{l}(\tau) = k_c \frac{\mu_0^{(1)}(\tau)}{\mu_0^{(0)}(\tau)} \quad (39)$$

is the Poisson mean.

Further, we define the coefficient of variation in particle radius (COV_{r_p}) as a measure toward the relative spread in the particle size distribution. It is the ratio of standard deviation to mean radius found from the model.

$$COV_{r_p}(\tau) = \frac{\{[\mu_1^{(2)}(\tau)/\mu_1^{(0)}(\tau)]^{1/3} - [\mu_1^{(1)}(\tau)/\mu_1^{(0)}(\tau)]^{2/3}\}^{1/2}}{[\mu_1^{(1)}(\tau)/\mu_1^{(0)}(\tau)]^{1/3}} \quad (40)$$

The authors[3] have however reported the standard deviation of the particle radius (σ_{r_p}) from their experiments. They have used a log-normal distribution for this purpose. We hence calculated their experimental coefficient of variation from the expression $(exp[\sigma_{r_p}^2] - 1)^{1/2}$ (which is known as the COV of a log-normal variable). This expression gave us the same value as the σ_{r_p} reported by

them. This value we compared with that obtained from our model (eq 40).

2.9. Initial Conditions. In the beginning, none of the micelles is nucleated and hence all moments related to nucleated micelles are zero. The mean number of $Ca(OH)_2$ molecules per micelle is calculated from the known amount of $Ca(OH)_2$ present in the micellar core and the number of micelles existing at the beginning of the experiment. The latter quantity is experimentally obtained by Roman et al.[3] Thus, the relevant set of initial conditions is as follows.

$$\mu_1^{(0)}(0) = 0 \quad (41)$$
$$\mu_1^{(1)}(0) = 0 \quad (42)$$
$$\mu_1^{(2)}(0) = 0 \quad (43)$$
$$\mu_0^{(0)}(0) = 1 \quad (44)$$
$$\mu_0^{(1)}(0) = 0 \quad (45)$$
$$\mu_{Ca(OH)_2}^{(1)}(0) = 5 \quad (46)$$
$$\mu_p^{(1,0)}(0) = 8.37 \times 10^9 \quad (47)$$

Because each micelle at $\tau = 0$ has 25 molecules of lime, the onset of phase II occurs when the solution shows $\mu_{Ca(OH)_2}^{(1)} = 0$, which happens when $\tau = 25$. This value of τ is independent of the values of q_m, q_p, k_g, or $k_n(l)$ we use. From this time onward, the equations differ, as discussed previously. The conditions at the end of phase I naturally form the initial conditions for phase II.

2.10. Nucleation Rate. Heterogeneous nuclei will not be present in the micelles in view of their small size and the absence of foreign bodies. The theory of the homogeneous nucleation rate can therefore be used. We use the expression for I, which is nucleation rate per unit volume from a condensed phase, quoted by Adamson[6] (originally derived by Turnbull and Fisher).

$$I = cA \exp\left(-\frac{\Delta G_{max}}{k_B T}\right) \quad (48)$$

ΔG_{max} is equal to one-third of the surface free energy of the nucleus, the expression for which has been given by Gibbs and is quoted by Adamson.[6]

$$\Delta G_{max} = \frac{16\pi\sigma^3 V_m^{\,2}}{3(k_B T)^2(\ln \lambda)^2} \quad (49)$$

In the above equation, λ is the supersaturation with respect to $CaCO_3$ and its value is dependent on the number of $CaCO_3(l)$ molecules present in a micelle. In a micelle containing l such molecules, it is given by

$$\lambda_l = \frac{[CaCO_3(l)]_l}{K_s^{1/2}} \quad (50)$$

where

$$[CaCO_3(l)]_l = \frac{l}{N_A V_{mic}} \quad (51)$$

(6) Adamson, A. W. *Physical Chemistry of Surfaces*; John Wiley & Sons: New York, 1990; p 369.

The nucleation rate $k_n(l)$ in a non-nucleated micelle containing l molecules of $CaCO_3(l)$ therefore is obtained by multiplying I from eq 48 with the volume of the micelle. However, c multiplied by the volume of the micelle is exactly equal to the number of $CaCO_3(l)$ molecules present in the non-nucleated micelle. Hence,

$$k_n(l) = IA \exp\left(-\frac{\Delta G_{max}}{k_B T}\right) \qquad (52)$$

with supersaturation being calculated from eq 50, corresponding to the prevailing concentration of l molecules of $CaCO_3(l)$ in the micelles.

For micelles of the size encountered in the experiments of Roman et al.,[3] the condition of supersaturation is attained even if one molecule of $CaCO_3(l)$ is present in a micelle. It would be unrealistic to expect a nucleus to form with just one $CaCO_3(l)$ molecule. Clearly, nucleation can be permitted only in those micelles which possess a minimum number of $CaCO_3(l)$ molecules required to form a nucleus. In our previous paper,[2] we had used a value of $k_c = 5$. We have retained the same value in the present work. On the basis of this consideration, the modified expression for the nucleation rate obtained from eqs 49 and 50 is the following.

$$k_n(l) = \begin{cases} 0, & l \leq 4 \\ IA \exp\left[-\frac{16\pi\sigma^3 V_m^2}{3(k_B T)^3 (\ln \lambda_l)^2}\right] & l \geq 5 \end{cases} \qquad (53)$$

Thus, eq 53 can be used to calculate the nucleation rate in conjunction with the moment equations.

2.11. Collision Frequency. We have used Brownian collision frequencies between three kinds of species: nucleated micelles (n), non-nucleated micelles (m), and lime particles (p). Among these, collisions among lime particles and between nucleated micelles themselves are inconsequential. This stems from the absence of any agglomeration of solid particles. In general, the collision frequency between species 1 and 2 given by Smoluchowski[7] is

$$q_{1-2} = \frac{2k_B T}{3\eta}\left[2 + \left(\frac{v_1}{v_2}\right)^{1/3} + \left(\frac{v_2}{v_1}\right)^{1/3}\right] \qquad (54)$$

where v_1 and v_2 are volumes of the colliding micelles or particles. The volume of a micelle is taken to be that corresponding to the reported initial micellar diameter. The volume of each nucleated micelle with time is also kept the same as the initial diameter, because the change in collision frequency, resulting from the growth of the particle inside, is only about 2%. Thus, for collision between equisized micelles (both m−m and m−n types) the above reduces to

$$q_m = \frac{8k_B T}{3\eta} \qquad (55)$$

For micellar collisions with lime particles (both m−p and n−p types), eq 54 is used, with initial diameters being used for simplicity. The coalescence efficiency between micelles and lime particles and among micelles themselves modifies the fusion rate and is described in the next section.

Table 2. Parameters for the Model of CaCO₃ Particle Formation in Overbasing

variable	value	variable	value
V_d	225.1 cm³	q_p	2.204×10^{-11} cm³ s⁻¹
$N_p^{(0)}(0)$	9.24×10^{10} cm⁻³	q_m	2.194×10^{-13} cm³ s⁻¹
$N_0^{(0)}(0)$	4.31×10^{18} cm⁻³	A	278.42 s⁻¹
β_p	0.055	k_c	5
β_m	7×10^{-6}	V_m	6.13×10^{-23} cm³
k_g	0.112 s⁻¹	σ	97 dyne cm⁻¹
k_B	1.3806×10^{-16} erg K⁻¹	V_{mic}	4.68×10^{-24} L⁻¹
η	0.50 P	K_s	3.31×10^{-12} mol² L⁻²
T	298 K		

3. Results and Discussion

3.1. Parameter Estimation. Computations have been carried up to 26 min, which is the duration of the experiments of Roman et al.[3] for obtaining stable, amorphous $CaCO_3$ nanoparticles. Toward this end, we solve eqs 26−31 for phase I and eqs 32−37 for phase II. The values of the various parameters are shown in Table 2.

Out of 26 g of lime initially present, 2.294 g goes toward reaction with sulfonic acid to generate the surfactant. The remaining lime particles are taken to be of size 1 μm (micron size range was mentioned by the authors), thereby giving a total of 2.08×10^{13} lime particles. These are dispersed in the dispersion of total volume, $V_d = 225.1$ cm³, calculated based on their data of volume of each component. Hence, the number density of lime particles is $N_p^{(0)} = 9.24 \times 10^{10}$ cm⁻³. From these particles, each micelle gets 25 molecules. The authors report a total of 9.7×10^{20} micelles in the dispersion, each of diameter 24.4 Å to start with. Thus there are $N_0^{(0)} = 4.31 \times 10^{18}$ micelles per cm³ of dispersion. Therefore at $t = 0$, the nondimensional number of lime particles to be used in the model equations given before is $\mu_p^{(0)} = 2.14 \times 10^{-8}$. Furthermore, $k_g = 0.112$ s⁻¹ has been used for the gas entry rate into micelles. As mentioned earlier, this value of k_g is evaluated from the experimental condition that all the sparged CO_2 is consumed[4] without any excess being left into the atmosphere. However, if gas is passed in excess, it will escape the system in the form of bubbles, and the method of calculation of k_g for using the present analysis under those circumstances is given in Appendix A. Also, the implications of the variation in sparging rate of CO_2 have been discussed in section 4.2 where simulation results are presented.

As was mentioned earlier, the coalescence efficiency between micelles and lime particles is evaluated from the experimentally fitted parameter β_p and works out to be 0.055. So is the case with β_m which also has been obtained to match the final results with experiments. The value of β_m turns out to be 7×10^{-6}. This is a rather low value. For example, the value of β_m for an AOT−water−cyclohexane system[8] is about 5×10^{-5}. However, the surfactant used by Roman et al.[3] has a tail consisting of alkyl groups and the solvent is xylene, which is aromatic in nature, and it is possible that the value of β_m may be lower. The viscosity of the medium η for use in eqs 54 and 55 is taken to be 0.50 P, as reported by Roman et al.[3] The coalescence frequencies were calculated from eqs 54 and 55 using the values of efficiencies discussed above and are listed in Table 2.

The nucleation rate $k_n(l)$ is obtained from eq 53. In eq 53, A is a pre-exponential factor and only a range of its

(7) Smoluchowski, M. V. *Phys. Z.* **1916**, *17*, 557.

(8) Flethcer, P. D. I.; Howe, A. M.; Robinson, B. H. *J. Chem. Soc., Faraday Trans. 1* **1987**, *83*, 985.
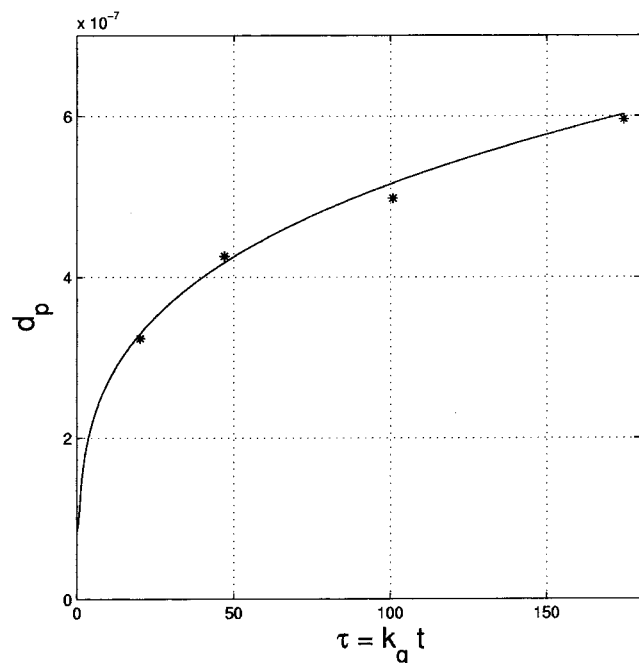
Figure 3. Comparison of experimental and model prediction of the temporal evolution of $CaCO_3$ particle diameter (d_p is in cm units).

values is available. In our previous paper (Bandyo-padhyaya et al.[2]), we fitted the parameter in this range, to quantitatively explain the experiments of Kandori et al.[1] We have retained the same value of 278.42 s^{-1} for predictions from the present model. The critical number of molecules has also been kept the same as in the previous paper, that is, $k_c = 5$. Other parameters, such as V_m and σ, required in eq 53, are specific to $CaCO_3$ and hence are taken from our previous paper.[2] The values are shown in Table 2. The micelles in the beginning contain mostly methanol and little water. A burst of nucleation is found to occur in a very short period after sparging begins, and nucleation occurs at a very slow rate thereafter. Hence, for the purposes of calculating supersaturation, we consider the micellar core to be purely methanol. The core volume to be used in eqs 51 and 53 is $V_{mic} = 4.68 \times 10^{-24}$ L. The solubility of sparingly soluble salts such as $CaCO_3$ is proportional to the cube of the dielectric constant of the solvent. Thus, we find that K_s in methanol (needed in eq 50) is 0.5% of K_s in water. The latter is 6.61×10^{-9} mol^2 L^{-2}. Thus, we have used $K_s = 3.31 \times 10^{-12}$ mol^2 L^{-2} in eq 50 for calculating supersaturation.

The population of non-nucleated micelles for higher values of l is small because $\bar{l}(t)$ generally does not reach up to the maximum value of 25 molecules because of rapid nucleation. Hence, in computations the sum appearing in eqs 26−37 has been truncated beyond $l = 50$.

3.2. Model Prediction. In predicting the experimental findings of Roman et al.,[3] we have first calculated the amount of lime present in each micelle in the beginning and used the experimentally reported CO_2 transfer rate, k_g. We have then solved the moment eqs 26−37 together.

Solution of the above equations also furnishes the number and evolution in the size of $CaCO_3$ particles with time, which are of principal interest. Figure 3 shows the variation in predicted diameter of a $CaCO_3$ particle (d_p) with time. The predicted size at all times compares very well with the experiments. Though the first experimental value reported is at 3 min ($\tau = k_g t = 20.2$), the sharpest evolution (nucleation and initial growth) occurs during phase I, for a duration of about 10 s ($\tau \sim 1$). Phase I
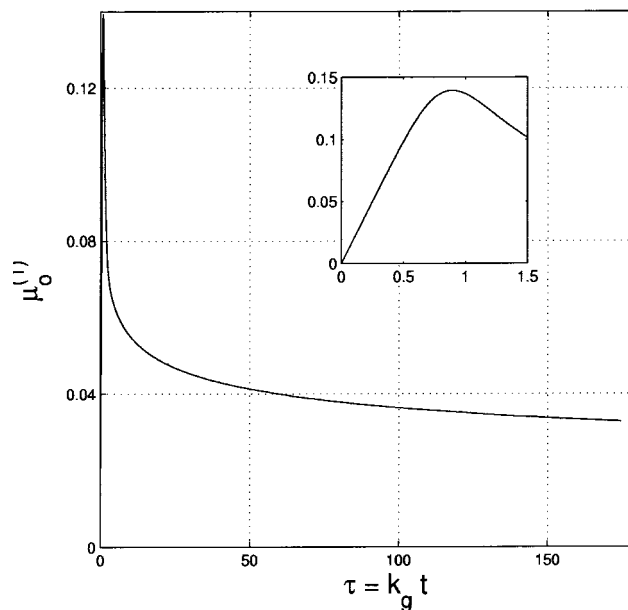

Figure 4. Variation in the nondimensional first moment of non-nucleated micelles. The inset shows the detail in the initial part of phase I.
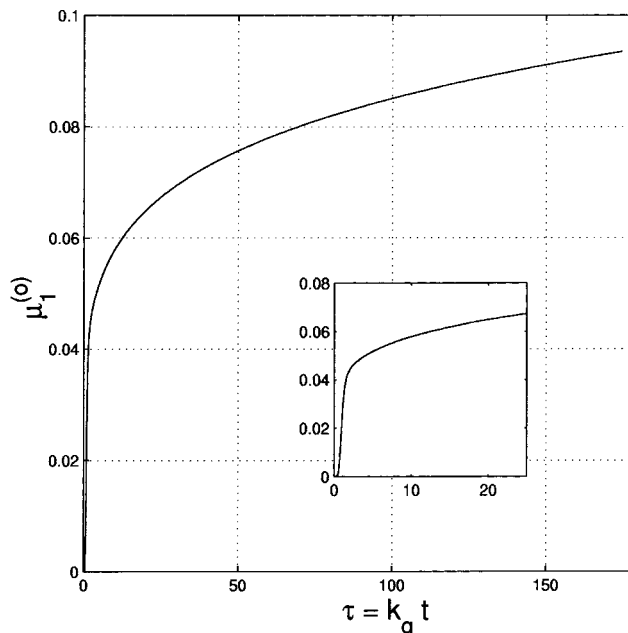

Figure 5. Variation in the nondimensional zeroth moment of nucleated micelles. The inset shows the detail in the initial part of phase I.

continues till the lime initially present in the micelles is exhausted ($\tau = 25$). Phase II then begins. The final predicted size is 60.2 Å at the end of 26 min, and the experimental measurement given in symbols (reported by Roman et al.[3]) indicates 59.6 Å, indicating close agreement between the two.

To explain how $CaCO_3(l)$ molecules build (by reaction) and decay (by nucleation and growth) with time and in turn influence nucleation, the moments $\mu_0^{(1)}$ and $\mu_1^{(0)}$ are plotted in Figures 4 and 5. Figure 4 shows that the mean number of molecules per micelle reached a maximum of only $0.14 \times l_c \sim 0.7$ molecules at $\tau \sim 1$ or at about 10 s. If nucleation did not occur, the mean number at this time should have been 1. Thus, nucleation occurs even before 10 s. Further, this implies that some micelles nucleate even though the mean occupancy is well below $k_c = 5$.
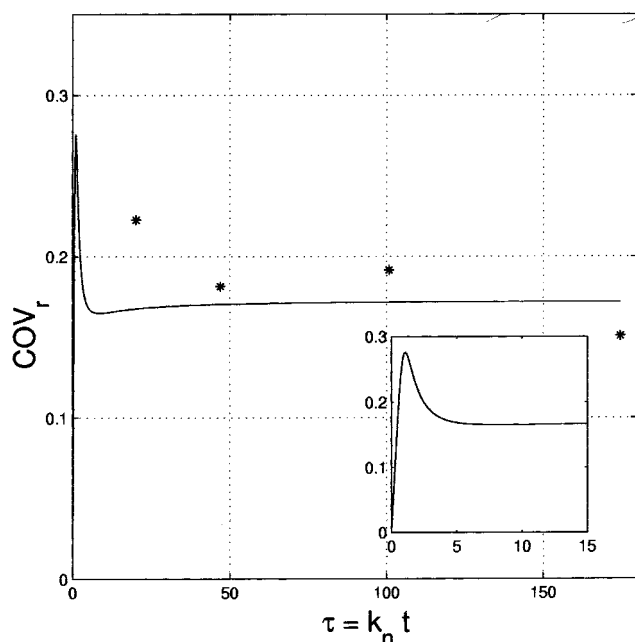
Figure 6. Comparison of experimental and model prediction of the temporal evolution in COV (coefficient of variation) of CaCO₃ particle radius. The inset shows the initial part of phase I.

This is due to the fact that the Poisson distribution creates a substantial number of micelles containing the critical number even when the mean occupancy is around unity. This is also confirmed from the plot of $\mu_1^{(0)}$ presented in Figure 5. It shows an initial burst of nucleation and that about 5% of the initially present micelles have nucleated in about 10 s. Subsequently also, CaCO₃(l) molecules continue to form. However, the CaCO₃(l) molecules are more rapidly absorbed by nanoparticles for their growth. Hence, there is a rapid decrease in the CaCO₃(l) molecules in the micelles as shown in Figure 4. Thus, the mean occupancy falls quickly to about 0.25 near the end of phase I and decreases further. Because of this, after the initial burst nucleation slows down. As can be seen from Figure 5, only about 2% more of the initially present micelles have nucleated by the end of phase I ($\tau \sim 1$), and another 2% more nucleate till the end of the process. Figure 5 shows that the number of nuclei reaches a value of 0.092, which compares well with the experimental value of 0.1. Thus, we conclude that about 10 micelles result in one CaCO₃ particle at the end. In other words, around 10% of the micelles nucleate.

The authors also present COV for different times and conclude that their values indicate nucleation over a very short time and constant growth thereafter. The COV values based on the model have been presented in Figure 6 along with the experimental values reported by the authors. It is seen that though there is a systematic deviation between experimental and predicted values in phase I, the trend in both the cases is the same. In each case, the COV decreases relatively sharply at low τ and tends to reach an asymptotic value toward the end of overbasing, there being very good agreement in this limiting value. Thus, the model captures the basic feature of the evolution of the distribution in particle radius.

The success of the model is not just in its ability to reproduce the experimental values and trends but in its ability to do so with the choice of the same parametric values for the nucleation pre-exponential factor (A) and critical number (k_c), obtained on an entirely different set

of data reported by Kandori et al.[1] The importance of the present model is then the generalized framework within which we have been able to closely predict the radically different number of particles obtained by Roman et al.[3] (10% of initial micelles) compared to the very small number of particles of Kandori et al.[1] (10^{-6}% of initial micelles).

Also of significance to us is to explore the principal reasons for such a huge orders of magnitude difference in the experimental results, as identified by the model. A high amount of lime initially present in the micelles encourages an increased extent of formation of CaCO₃(l) *per micelle*. In contrast, the lime population in micelles was very low (<0.1) in the work of Kandori et al.[1] The higher population of carbonate molecules in the experiments of Roman et al.[3] translates into a very high fraction of micelles that can nucleate. The presence of methanol in the micellar core reduces the solubility of carbonate even further, making nucleation more facile. Moreover, the medium used by Roman et al.[3] is about 55 times more viscous, thus reducing intermicellar exchange frequency and hence particle growth.

4. Implications of Rate of Gas Transfer

Instantaneous Gas Transfer Rate. The present model has been based on time scale analysis, relevant to the experimental conditions of Roman et al.[3] Rapid nucleation has been possible primarily because of the presence of a large number of Ca(OH)₂ molecules initially in the micelles. In fact, the formation of CaCO₃(l) molecules was limited by the availability of CO₂. It may be possible to obtain even higher rates of nucleation if CO₂ could be pumped into the micelles at still higher rates. This may be realized in practice by (i) sparging gas in excess such that bubbles leave the reaction mixture (dealt with in the Appendix), (ii) using high pressure to increase the concentration gradient, and (iii) increasing the gas–liquid interfacial area through the use of better contactors. Matson et al.[9] have prepared Al(OH)₃ particles by injecting ammonia in the continuous phase of supercritical propane. The AOT reverse micelles in propane had predissolved Al(NO₃)₂ solution. They have speculated that operation in the supercritical fluid regime may allow high mass transfer rates of reactants (in this case ammonia) to and across the micelles and should relax rate limitations when one of the reactants is a gas.

The calculation presented in the Appendix shows that even under atmospheric pressure, if gas is passed in excess the value of k_g is of the order of 2300 s^{-1}. It is 23 000 times more than the rate at which the gas was made available in the experiments of Roman et al.[3] Hence, as an extreme case we analyze the implications of instantaneous CO₂ transfer into the micelles. Nucleation now takes place only after all micelles have acquired 25 CaCO₃(l) molecules by instantaneous CO₂ transfer and reaction, rendering the initial nucleation rate for the micelles to be equal. However, micelles containing only water are generated by fusion of nucleated and supersaturated micelles and through subsequent fission of the dimer. Initially at least, the water micelles will constitute only a small fraction of the population. If we neglect the collisions of these water micelles with the supersaturated ones until all the supersaturation corresponding to the initial lime content is exhausted via nucleation or by fusion with nucleated micelles, we obtain an analytical solution to the number of particles.

(9) Matson, D. W.; Fulton, J. L.; Smith, R. D. *Mater. Lett.* **1987**, *6*, 31.

On the basis of the two steps of nucleation and collision–fusion discussed above, the zeroth moments of non-nucleated and nucleated micelles are written as follows.

$$\frac{dN_0^{(0)}(t)}{dt} = -k_n(25)\,N_0^{(0)}(t) - \beta_m q_m N_1^{(0)}(t)\,N_0^{(0)}(t) \quad (56)$$

$$\frac{dN_1^{(0)}(t)}{dt} = k_n(25)\,N_0^{(0)}(t) \quad (57)$$

Now dividing both sides of eqs 56 and 57 by $k_n(25)$ $N_0^{(0)}(0)$, we obtain the nondimensional moments. These are

$$\frac{d\mu_0^{(0)}}{d\tau'} = -\mu_0^{(0)}(\tau') - \Omega(25)\,\mu_1^{(0)}(\tau')\,\mu_0^{(0)}(\tau') \quad (58)$$

$$\frac{d\mu_1^{(0)}}{d\tau'} = \mu_0^{(0)}(\tau') \quad (59)$$

where

$$\tau' = k_n(25)t \quad (60)$$

and

$$\Omega(25) = \frac{\beta_m q_m N_0^{(0)}(0)}{k_n(25)} \quad (61)$$

The analytical solution derived from the coupled nonlinear eqs 58 and 59 is

$$\mu_1^{(0)}(\tau') = \mu_1^{(0)+} + \frac{2\sqrt{1+2\Omega(25)}}{\Omega(25)} \times$$

$$\frac{\mu_1^{(0)+}\exp(-\tau'\sqrt{1+2\Omega(25)})}{\mu_1^{(0)-} - \mu_1^{(0)+}\exp(-\tau'\sqrt{1+2\Omega(25)})} \quad (62)$$

where

$$\mu_1^{(0)\pm} = -\frac{1}{\Omega(25)}[1 \mp \sqrt{1+2\Omega(25)}] \quad (63)$$

In the limit of large times ($\tau' \to \infty$), from eq 62 we find $\mu_1^{(0)}(\tau_f) = \mu_1^{(0)+}$. The ratio of the final number of particles to the initial number of micelles therefore is

$$\mu_1^{(0)}(\tau_f) = \frac{\sqrt{1+2\Omega(25)}-1}{\Omega(25)} \quad (64)$$

The analytical solution brings out the relative importance of collision and nucleation rates on particle formation, in terms of the nondimensional parameter $\Omega(25)$ defined in eq 61. Thus, the higher the ratio, the smaller the nucleation rate and hence the number of particles. Hence, if $\Omega(25) > 1$ then all micelles would not nucleate.

With the micelle–micelle collision frequency $q_m = 2.194 \times 10^{-13}$ cm^3 s^{-1}, the intermicellar coalescence efficiency $\beta_m = 7 \times 10^{-6}$, and the nucleation rate in methanol $k_n(25) = 119.2$ s^{-1}, we obtain $\Omega(25) = 0.056$. Equation 64 then gives the desired ratio to be 0.973, indicating 97.3% of micelles can nucleate. Thus, the limiting analysis shows that an increase in the sparging rate and/or pressure in the vessel can indeed help in producing still larger numbers of particles, from 10% obtained in experiments to a maximum of 97.3% of initial micelles. The particles would necessarily be smaller as the total amount of product is the same. Knowing the initial amount of lime, one can then estimate the CaCO$_3$ particle size. The approximate solution provided by eq 64 is therefore of interest. We can estimate the maximum number of nanoparticles and hence the smallest size that can be synthesized with very high CO$_2$ transport. On the other hand, for a particular size requirement one can a priori specify the range of values of some key experimental conditions required to be followed.

In the limit of instantaneous gas transfer and reaction, the process of Kandori et al.[1] also reduces to the present analysis. The differences in their experiments are the following. The lime present initially in a dissolved form being very scarce, the CaCO$_3$(l) molecules are distributed in a Poisson manner, and the intermicellar coalescence efficiency varies from 10% to 0.5% depending on R. When $\Omega \gg 1$, as in their experiment, the limiting form of eq 64 is $\sqrt{1/\Omega}$. For their experiment, we define

$$\Omega_k = \frac{\beta_m q_m N_0^{(0)}(0)(1-P_0)}{k_n(k_c)P_{k_c}} \quad (65)$$

The numerator gives the rate at which a particle in a nucleated micelle undergoes fusion–growth due to collisions with supersaturated micelles. The term $(1 - P_0)$ gives the fraction of the supersaturated micelles, that is, those containing one or more molecules. The denominator is a product of the intrinsic nucleation rate of a micelle having k_c number of CaCO$_3$(l) molecules with the fraction of such micelles, thus giving the average rate with which a non-nucleated micelle can nucleate. Hence, $\Omega_k(k_c)$ is a measure of the relative rates of the two steps that we consider in the simplified analysis. We find that for $k_c = 5$, our calculated value of Ω_k for their process is $\sim 10^{14}$. Thus, the ratio $\sqrt{1/\Omega_k}$ is 10^{-7}, which is close to the order of 10^{-8}, found in the experiments of Kandori et al.[1]

Effect of Sparging Rate. If gas is sparged at a rate smaller than that calculated in the Appendix, all of it will be absorbed and none of it will escape in the form of bubbles as in the experiments of Roman et al.[3] In such a case, the value of k_g is simply given by the flow rate of gas in molecules per second divided by the number of micelles in the system, the latter being equal to 9.7×10^{20}. As the value of k_g is increased, the rate of formation of CaCO$_3$(l) increases, and hence the mean occupancy also increases. As argued in the previous section, this in turn leads to the formation of a greater number of nuclei and, in view of the fixed amount of lime available, a smaller particle size. This is shown in Figure 7, keeping all the other parameters in the model constant. Curve C shows the results for $k_g = 10$, and curve B shows the results for $k_g = 0.224$. It can be seen that the particle size is reduced significantly in the former case. The particle size decreases significantly only when nucleation can dominate growth by collision–fusion. This in turn can occur only when the mean population of CaCO$_3$(l) can be raised more rapidly than can be consumed by collisional growth. The ratio of the rates of these two processes is k_g/τ_{cn}^{-1} and is about 0.1 for the condition of Roman et al.[3] ($k_g \sim 0.1$). Thus, significant changes in the final particle size cannot be expected till the ratio exceeds 1, as with curve C of Figure 7.

The above discussion has certain practical implications for the conduct of the overbasing process. If during sparging of CO$_2$ significant unevenness in the availability of CO$_2$ to micelles is created because of poor mixing, it would affect the final particle size considerably.
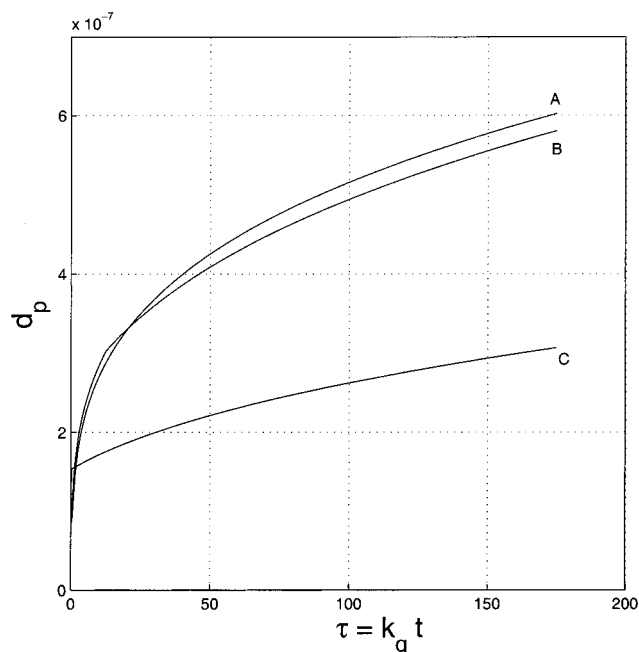
Figure 7. The effect of sparging rate of CO_2 on particle diameter shown in cm units. The top curve (A) is for $k_g = 0.112$ s^{-1}, the middle curve (B) is for $k_g = 0.224$ s^{-1}, and the bottom curve (C) is for $k_g = 10$ s^{-1}.

5. Conclusions

During the formation of nanoparticles through swollen reverse micelles, nucleation based on supersaturation and growth based on Brownian collisions decide both the numbers and the size distribution of the particles. Though mass transfer, reaction, nucleation, growth, and collisions occur simultaneously, a comparison of various time scales can lead to models in which processes occur sequentially and hence can be analyzed easily. It is seen that a framework of population balance equations obtained through the application of time scale analysis is able to explain results of the carbonation of lime, which differ by many orders of magnitude.

Though tested for carbonation of lime, the model is quite general and is applicable to situations where gas–liquid reactions yield nanoparticles in a fashion such that growth time scales are much lower than nucleation and collision time scales.

Roman et al.[3] also make an interesting observation in their paper that if carbonation is carried out further up to about 40 min, the dispersion becomes unstable. They attribute this to crystallization of CaCO₃. The model presented does not address morphological issues, and further work is needed in this direction to be able to explain the observed effect.

Appendix

Calculation of CO₂ Transfer Rate at High Sparging Rates. In this Appendix, we calculate the maximum gas input rate to the micelles at atmospheric pressure. To this end, gas is assumed to be sparged at such a rate that the excess CO₂ escapes from the reaction mixture in the form of bubbles. We use the penetration theory formalism to calculate the rate of transfer of CO₂. CO₂ diffuses from

the gas bubbles into the organic solvent and then into the micelles. The thickness of the diffusion layer around the bubbles is of the order of a micron. The micelles are very small and hence will be present in the diffusion layer itself. As the bubbles are large compared to the diffusion layer thickness, we can treat the gas–liquid interface as planar. Consider CO_2 (A) diffusing from a planar interface into a semi-infinite organic medium. The interface at $x = 0$ is maintained at a saturation concentration of C_{A_0}. A is absorbed into the micelles where it reacts with $Ca(OH)_2$ (B) present in excess. As this reaction is instantaneous, the rate of absorption of A into a single micelle is given by $(2D/d_m)(\pi d_m^2/4)C_A$. Thus, the equation for diffusion of A in the organic medium is given by

$$\frac{\partial C_A}{\partial t} = D\frac{\partial^2 C_A}{\partial x^2} - K'C_A \tag{A1}$$

where

$$K' = \frac{2D}{d_m}\frac{N_t}{V_d}\frac{\pi d_m^2}{4} \tag{A2}$$

Here, $D = 10^{-5}$ cm^2 s^{-1} is the diffusivity of CO_2 in the organic medium, $N_t = 9.7 \times 10^{20}$ is the total number of micelles in dispersion, $d_m = 24.4 \times 10^{-8}$ cm is the diameter of micelle, and $V_d = 225.1$ cm^3 is the total volume of dispersion. Hence, $K' = 1.65 \times 10^7$ s^{-1}.

The relevant initial and boundary conditions are given by

$$t = 0 \qquad C_A = 0$$
$$x = 0 \qquad C_A = C_{A_0}$$
$$x = \infty \qquad C_A = 0$$

Bird et al.[10] give a solution of eq A1 and an expression for moles of A absorbed (M_A) through unit gas–liquid contact area, between $t = 0$ and t_0. As $K't_0 \gg 1$, we use the simplified expression given for this condition.

$$M_A = \sqrt{DK'}\,C_{A_0}\left(t_0 + \frac{1}{2K'}\right) \tag{A3}$$

For large K', as we have found here, the mass transfer rate of A (i.e., CO_2) is hence

$$\frac{d[CO_2]}{dt} = \sqrt{DK'}\,a_{g-1}C_{A_0} \tag{A4}$$

where $a_{g-1} = 15$ cm^2/cm^3 is the maximum gas–liquid interfacial area in mechanically stirred gas in liquid dispersion (Doraiswamy and Sharma[11]) and C_{A_0} is the saturation concentration of CO_2 in the organic phase and is[12] 0.085 mol L^{-1}. The right-hand side of eq A4 gives the CO_2 mass transfer rate to be 16.38 mol L^{-1} s^{-1}. The number of CO_2 molecules entering per micelle per second is therefore obtained by multiplying it with $N_A V_d/(1000\,N_t)$, giving the CO_2 entry rate into a micelle as $k_g = 2289$ s^{-1}. This corresponds to passing CO_2 at a rate of 220 mol/min, a rate that may be difficult to reach in practice. Further, as mentioned in the main text, if gas is passed at a rate

(10) Bird, R. B.; Stewart, W. E.; Lightfoot, E. N. *Transport Phenomena*; John Wiley & Sons: New York, 1960; p 621.
(11) Doraiswamy, L. K.; Sharma, M. M. *Heterogeneous Reactions*; John Wiley & Sons: New York, 1984; Vol. 2, p 330.
(12) Just, G. Z. *Phys. Chem.* **1901**, *37*, 342.

less than that calculated above (74.95 mol L^{-1} s^{-1} or $k_g =$ 2289 s^{-1}), all the sparged gas is expected to dissolve, as is the case with the sparging rate used by Roman.[4]

Nomenclature

A	Pre-exponential factor in nucleation rate, s^{-1}
[CaCO$_3$(l)]	Molar concentration of CaCO$_3$(l) in micellar core, mol L^{-1}
COV	Coefficient of variation
c	Number concentration of any species in micellar core, cm^{-3}
I	Nucleation rate from condensed phase, cm^{-3} s^{-1}
i	Number of Ca(OH)$_2$ molecules in a micelle
j	Number of CO$_2$ molecules in a micelle
K_s	Solubility product of CaCO$_3$, mol^2 L^{-2}
k	Number of CaCO$_3$ molecules in a particle inside a micelle
k_B	Boltzmann constant, 1.3806 × 10^{-16} erg K^{-1}
k_c	Critical number of CaCO$_3$(l) molecules required in a micelle for nucleation
k_g	Entry rate of number of CO$_2$ molecules into a micelle, s^{-1}
$k_n(l)$	Homogeneous nucleation rate in a micelle containing l CaCO$_3$(l) molecules, s^{-1}
k_1	Rate constant of reaction between CO$_2$ and OH^{-1}, L mol^{-1} s^{-1}
l	Number of CaCO$_3$(l) molecules in a non-nucleated micelle
$\bar{l}$	Mean number of CaCO$_3$(l) molecules in a non-nucleated micelle
N_A	Avogadro's number, 6.023 × 10^{23} mol^{-1}
$N_{Ca(OH)_2}^{(1)}$	Total number of Ca(OH)$_2$ molecules in all micelles per unit volume of dispersion, cm^{-3}
$N_p^{(0)}$	Number of suspended lime particles per unit volume of dispersion, cm^{-3}
$N_p^{(1)}$	Total number of Ca(OH)$_2$ molecules in suspended lime particles per unit volume of dispersion, cm^{-3}
$N_0^{(n)}$	nth moment of non-nucleated micelle population per unit volume of dispersion, cm^{-3}
$N_0^{(0)}$	Total number of non-nucleated micelles per unit volume of dispersion, cm^{-3}
$N_0^{(0)}(0)$	Total number of micelles present in the beginning per unit volume of dispersion, cm^{-3}
$N_0^{(1)}$	Total number of CaCO$_3$(l) molecules in non-nucleated micelles per unit volume of dispersion, cm^{-3}
$N_0^{(2)}$	Second moment of CaCO$_3$(l) population in non-nucleated micelles per unit volume of dispersion, cm^{-3}
$N_1^{(n)}$	nth moment of nucleated micelle population per unit volume of dispersion, cm^{-3}
$N_1^{(0)}$	Total number of nucleated micelles per unit volume of dispersion, cm^{-3}
$N_1^{(1)}$	Total number of CaCO$_3$ molecules in nucleated micelles per unit volume of dispersion, cm^{-3}
$N_1^{(2)}$	Second moment of CaCO$_3$ population in nucleated micelles per unit volume of dispersion, cm^{-3}
$n_0(l, t)$	Number of non-nucleated micelles per unit volume of dispersion containing l molecules of CaCO$_3$(l), cm^{-3}
$\bar{n}_0(l, \tau)$	Scaled number of non-nucleated micelles containing l molecules of CaCO$_3$(l)
$n_1(k, \tau)$	Number of nucleated micelles per unit volume of dispersion containing k molecules of CaCO$_3$, cm^{-3}
$\bar{n}_1(k, \tau)$	Scaled number of nucleated micelles containing k molecules in the CaCO$_3$ particle
P_l	Probability of a micelle containing l molecules of CaCO$_3$(l)
q	Brownian collision frequency between nucleus and solute molecules in micellar core, cm^3 s^{-1}
q_m	Brownian collision frequency between micelles, cm^3 s^{-1}
q_p	Brownian collision frequency between micelles and lime particles, cm^3 s^{-1}
R	Molar ratio of dispersed phase (water and methanol) to surfactant
T	Temperature of experiment, 298 K
t	Time, s
V_d	Volume of the entire system, cm^3
V_m	Volume of a CaCO$_3$ (calcite) molecule, 6.1265 × 10^{-23} cm^3
V_{mic}	Volume of micellar core, L

Greek Symbols

β_m	Coalescence efficiency in intermicellar collisions
β_p	Coalescence efficiency in micelle−particle collisions
ΔG_{max}	Maximum free energy change during nucleation, erg
$\zeta(l)$	Nondimensional ratio of nucleation rate in a micelle (for lCaCO$_3$(l) molecules) to CO$_2$ entry rate
η	Viscosity of continuous organic medium, 0.009 g cm^{-1} s^{-1}
λ_l	Supersaturation due to l molecules of any sparingly soluble salt
$\mu_{Ca(OH)_2}^{(1)}$	Scaled number of Ca(OH)$_2$ molecules in all micelles
$\mu_p^{(0)}$	Scaled number of suspended lime particles
$\mu_p^{(1)}$	Scaled number of Ca(OH)$_2$ molecules in suspended lime particles
$\mu_p^{(1,0)}$	Mean number of Ca(OH)$_2$ molecules in any suspended lime particle
$\mu_0^{(n)}$	nth nondimensional moment of non-nucleated micelle population per unit volume of dispersion
$\mu_1^{(n)}$	nth nondimensional moment of nucleated micelle population per unit volume of dispersion
σ	Interfacial tension between nucleus and micellar core liquid, 97 dyne cm^{-1}
τ	Nondimensional time based on k_g
τ_S	Time scale of a micellar event with subscript S, s
τ'	Nondimensional time based on k_n
$\Omega(k_c)$	Nondimensional ratio of coalescence rate of a given micelle with another micelle to its own nucleation rate (for k_c CaCO$_3$(l) molecules)
$\Omega(25)$	Nondimensional ratio of coalescence rate of a given micelle with another micelle to its own nucleation rate (for 25 CaCO$_3$(l) molecules)
$\Omega_k(k_c)$	Same nondimensional ratio as above, defined for Kandori et al.'s experiment
$\Omega_p(k_c)$	Nondimensional ratio of coalescence rate of a given micelle with a lime particle to its own nucleation rate (for k_c CaCO$_3$(l) molecules)

Subscripts

c	Coalescence with any micelle
cb	Coalescence with a blank micelle
cn	Coalescence with a nucleated micelle
cp	Coalescence with lime particle

g	Growth of particle inside micelle
m	Mass transfer of CO_2 into micelle
n	Nucleation in a single micelle
nn	Nucleation in any micelle in the medium
p	Lime particle
r	Reaction in a micelle
0	Non-nucleated micelle
1	Nucleated micelle

Superscripts

(m)	Methanol
(n)	nth moment of the distribution
(0)	Zeroth moment
(1)	First moment
(2)	Second moment